NEUROSCIENCE

Neurite architecture of the planum temporale predicts neurophysiological processing of auditory speech

Sebastian Ocklenburg[1]*†, Patrick Friedrich[1]†, Christoph Fraenz[1]†, Caroline Schlüter[1], Christian Beste[2], Onur Güntürkün[1], Erhan Genç[1]

Copyright © 2018 The Authors, some rights reserved; exclusive licensee American Association for the Advancement of Science. No claim to original U.S. Government Works. Distributed under a Creative Commons Attribution NonCommercial License 4.0 (CC BY-NC).

The left hemispheric advantage in speech perception is reflected in faster neurophysiological processing. On the basis of postmortem data, it has been suggested that asymmetries in the organization of the intrinsic microcircuitry of the posterior temporal lobe may produce this leftward timing advantage. However, whether this hypothetical structure-function relationship exists in vivo has never been empirically validated. To test this assumption, we used in vivo neurite orientation dispersion and density imaging to quantify microcircuitry in terms of axon and dendrite complexity of the left and right planum temporale in 98 individuals. We found that a higher density of dendrites and axons in the temporal speech area is associated with faster neurophysiological processing of auditory speech, as reflected by electroencephalography. Our results imply that a higher density and higher number of synaptic contacts in the left posterior temporal lobe increase temporal precision and decrease latency of neurophysiological processes in this brain region.

INTRODUCTION

Auditory speech processing involves the posterior temporal cortex and is strongly left-lateralized in most individuals (*1*–*5*). Possibly, a key difference that drives left hemispheric language dominance is the time advantage and the higher temporal resolution of the left hemisphere (*6*). The planum temporale (PT), a brain area on the surface of the posterior superior temporal gyrus, likely plays an essential role for leftward functional asymmetries in the language system (*7*). Postmortem analyses show that the left PT not only is larger than the right PT (*8*, *9*) but also is characterized by a larger number of functionally coupled and densely innervated columnar neuronal units (*10*–*14*). These morphological left-right differences could be related to the left hemispheric time advantage. Unfortunately, detailed in vivo knowledge about the cellular morphological asymmetries of the PT and their relation to faster left hemispheric speech processing in a sufficiently large number of subjects is missing up to now, especially regarding the underlying neurophysiological process, for example, as reflected by asymmetries in electroencephalography (EEG) measures. Without these insights, however, it is impossible to deduce how lateralized network properties translate into hemispheric language dominance.

Up to now, it was impossible to fill this gap due to a lack of practical in vivo methods to examine the microstructural layout of the temporal cortex on the level of axons or dendrites. The introduction of NODDI (neurite orientation dispersion and density imaging), which enables the magnetic resonance imaging (MRI)–based quantification of neurite morphology, has resolved this problem. NODDI uses a multishell high-angular-resolution diffusion imaging protocol and offers a novel way to analyze diffusion-weighted data with regard to tissue microstructure in white and gray matter. The technique features a three-compartment model distinguishing intraneurite, extraneurite, and cerebrospinal fluid environments.

[1]Institute of Cognitive Neuroscience, Biopsychology, Department of Psychology, Ruhr-University Bochum, Universitätsstrasse 150, 44780 Bochum, Germany. [2]Cognitive Neurophysiology, Department of Child and Adolescent Psychiatry, Faculty of Medicine, TU Dresden, Fetscherstrasse 74, 01307 Dresden, Germany.
*Corresponding author. Email: sebastian.ocklenburg@rub.de
†These authors contributed equally to this work.

NODDI is an in vivo imaging approach based on a simplified version of a more complex diffusion model that was successfully validated by histological examinations using staining methods in the gray and white matter of mammals (*15*, *16*). Cortical gray matter, for the most part, is composed of somata and neuropil, namely, dendrites, axons, and glial cell processes that restrict the movement of water molecules. The density and geometric orientation of the dendritic and axonal stick-like diffusion patterns bring four NODDI markers, which point to a quantitative estimate of neurite density and neurite orientation dispersion (*15*–*17*). Furthermore, cortical gray matter also includes glial cells and blood vessels that cause a hindered pattern of water diffusion, which is used to estimate cell density in NODDI. Histological examinations show that the relative proportion of glial cells and blood vessels within a fixed volume of the cortex is relatively small compared to other components (*18*). As a consequence, the diffusion signals of NODDI metrics are mainly shaped by the architecture of neurites and somata (*15*, *16*). It was recently demonstrated that NODDI is capable of estimating diffusion markers of neurite density and orientation dispersion by in vivo measurements in humans (*17*). NODDI makes it possible that neurophysiological and microstructural analyses are conducted with the same subject. Direct validation of NODDI has recently been performed in a study investigating neurite dispersion as a potential marker of multiple sclerosis pathology in postmortem spinal cord specimens (*19*). They reported that neurite density obtained from NODDI significantly matched neurite density, orientation dispersion, and myelin density obtained from histology. Furthermore, the authors also found that NODDI neurite dispersion matched the histological neurite dispersion. This indicates that NODDI metrics closely reflect their histological conditions.

Here, we present the first in vivo examination of the microstructural neurite architecture of the human PT and its relation to the neurophysiology of auditory speech perception. We obtained NODDI images from a large sample of healthy participants (N = 98; mean age, 23.62 years; SD, 3.58; 52 males, 46 females). We compared macro- and microstructural brain properties of the PT across the hemispheres and examined their relationship with the neurophysiological correlates of lateralized auditory speech perception. We

hypothesize that microstructural neurite PT asymmetries as measured with NODDI will predict leftward functional hemispheric asymmetries in the neurophysiological correlates of auditory speech perception. As it has been suggested that the enhanced temporal resolution and speed of Wernicke's area in the left hemisphere underlie functional leftward dominance for auditory speech perception (*6*), we used EEG to assess lateralization of the N1 event-related potential (ERP) component, the earliest reliable leftward lateralized neurophysiological correlate of auditory speech perception. To this end, we used a verbal dichotic listening paradigm. The N1 is an early negative ERP component that shows a pronounced leftward lateralization at posterior electrode sites for verbal stimuli (*20*). It is the earliest ERP component that is associated with verbal recognition (*21*) and is thought to reflect orientation of attention toward a stimulus (*22*). Possibly, the left lateralization of the N1 after presentation of verbal stimuli reflects the greater effectiveness of the left hemisphere when processing verbal stimuli (*20*).

RESULTS

Figure 1A shows the EEG results of the dichotic and noise condition for the chosen electrodes. For amplitudes, the ANOVA (analysis of variance) showed a significant main effect of condition ($F_{1,97} = 281.81$; $P < 0.001$; $\eta^2 p = 0.74$), indicating a more negative N1 amplitude in the dichotic condition (−2.52 ± 0.11 μV) than in the noise condition (−0.50 ± 0.06 μV). All other effects failed to reach significance (all $P > 0.66$).

For the latencies, the ANOVA yielded a significant main effect of hemisphere ($F_{1,97} = 12.45$; $P < 0.001$; $\eta^2 p = 0.11$), showing an earlier N1 peak onset in the left hemisphere (111 ± 1.11 ms) than in the right hemisphere (119 ± 1.07 ms). In addition, the main effect of condition reached significance ($F_{1,97} = 17.35$; $P < 0.001$; $\eta^2 p = 0.11$). Comparison of the conditions revealed that the average N1 peak onset was faster in the noise condition (111 ± 1.15 ms) than in the dichotic condition (118 ± 0.99 ms). The key interaction hemisphere × condition was significant ($F_{1,97} = 14.25$; $P < 0.001$; $\eta^2 p = 0.09$). Bonferroni-corrected post hoc tests indicated significant hemispheric asymmetries in the dichotic condition ($P < 0.001$). Here, an earlier N1 peak onset was observed in the left hemisphere (112 ± 1.37ms) compared to the right hemisphere (125 ± 1.33 ms). In the noise condition, there were no significant hemispheric asymmetries in N1 latencies ($P > 0.82$). Thus, in line with previous literature, we found a leftward lateralization of the N1 for speech stimuli.

To estimate the cortical distribution of the sources generating the N1, we used standardized low-resolution brain electromagnetic tomography (sLORETA) (*23*). A one-sample *t* test [corrected for multiple comparisons using statistical nonparametric mapping (SnPM), $P < 0.01$] was calculated for the dichotic condition. This test indicated that N1 differences between the conditions were due to activation differences in the superior temporal lobe. The predominant source was the PT in the superior temporal gyrus (BA41/BA42) of the left hemisphere (Fig. 1B). Thus, sLORETA analysis (*24*) revealed that the left PT was the main source of N1 differences.

On the basis of the sLORETA results, we then investigated the microstructural properties of the PT using NODDI imaging. This was done to test whether specific microstructural properties of the PT are associated with our neurophysiological outcome measure. To quantify microstructural properties in terms of the axonal and dendritic density in the PT, we determined the so-called intraneurite volume fraction (INVF) in the left and right PT (see Fig. 2 and Materials and Methods for a detailed description of the measure).

In addition, dendritic arborization was determined using the neurite orientation dispersion index (ODI) (see Fig. 2 and Materials and Methods for a detailed description of the measure). Moreover, we determined the isotropic diffusion (ISO) as a control measure for water diffusion in cerebrospinal fluid.

For the first time, our study provides strong empirical evidence for leftward structural asymmetries in PT neurite architecture in vivo. We found significant left-right differences for two NODDI in vivo measures of PT microstructure. The INVF of the left PT (0.33 ± 0.01) was significantly higher than that of the right PT (0.32 ± 0.02) ($t_{97} = 5.27$; $P < 0.001$). INVF is a marker of neurite density. Thus, the significant leftward asymmetry we observed for neurite density indicates a higher concentration of dendrites and axons in the gray matter of the left PT than of the right PT. Furthermore, the ODI of the left PT (0.58 ± 0.03) was significantly higher than that of the right PT (0.56 ± 0.03) ($t_{97} = 4.53$; $P < 0.001$), indicating a leftward asymmetry of dendritic arborizations in the PT. In contrast, ISO did not show hemispheric differences between the left PT (0.19 ± 0.04) and the right PT (0.19 ± 0.05) ($t_{97} = -0.19$; $P = 0.85$). Thus, there were no systematic structural diffusion differences between the left

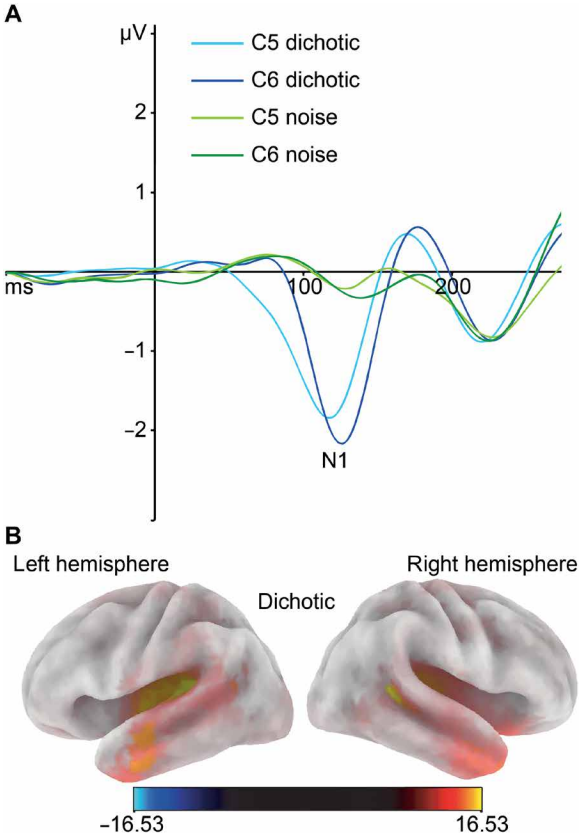

Fig. 1. Neurophysiological results for ERPs and sLORETA. (**A**) Averaged ERP waveforms for left (C5) and right (C6) electrodes. Blue tones represent the dichotic condition. Green tones represent the noise condition. (**B**) Source localization of the dichotic condition. sLORETA was used to show the cortical distribution of activation during the peak onset of the N1 component of the dichotic condition. Warm colors reflect positive current source density.

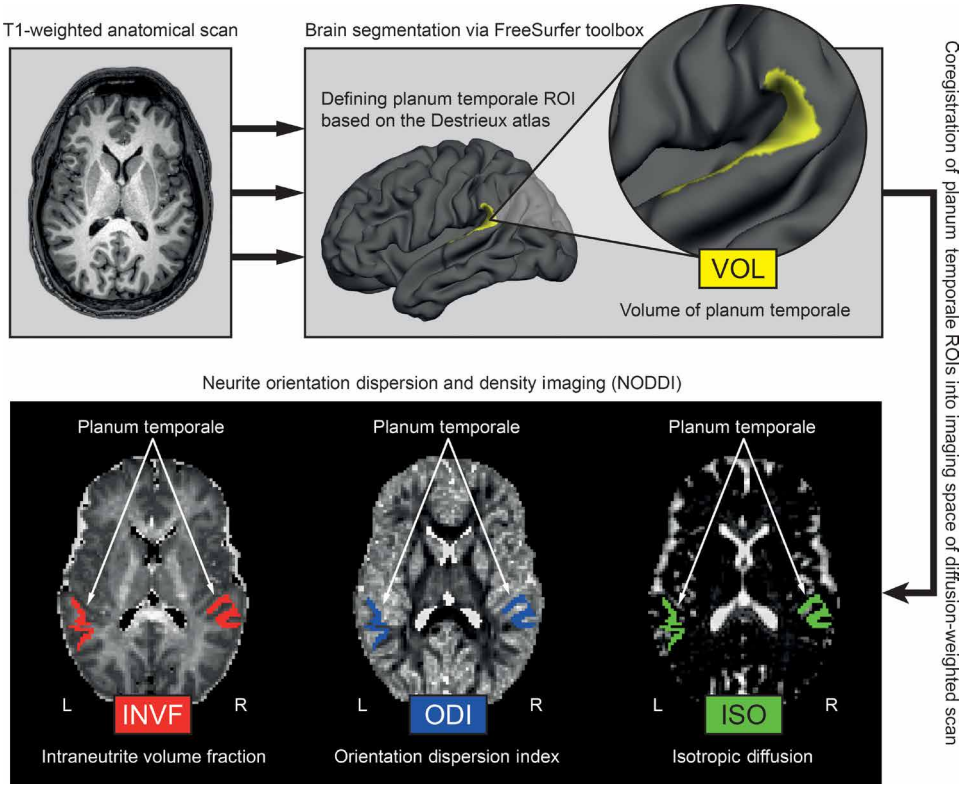

Fig. 2. Methodological sequence for the estimation of brain properties. T1-weighted images were automatically segmented into gray and white matter using surface-based methods in FreeSurfer (top left). From the reconstructed cortical surface, the PT in each hemisphere was defined according to the Destrieux atlas (top right) and volume estimates (VOL) were obtained. The PT was linearly transformed into the native space of the diffusion-weighted NODDI images, and different microstructural measures (INVF, ODI, and ISO) were computed (bottom). ROIs, regions of interest.

and the right PT, but there were specific differences in neurite architecture.

To contrast microstructural properties of the PT to its macrostructure of the PT, we then determined the PT volume (VOL) in the left and the right hemisphere. This was done as the macrostructural leftward asymmetry of the PT has been suggested to underlie functional lateralization (*25*). As expected, we found a significant macroscopic volume difference for the PT between the two hemispheres. On average, the volume of the left PT (2081 ± 460 mm^3) was significantly larger than that of the right PT (1645 ± 330 mm^3) ($t_{97} = 11.01$; $P < 0.001$).

Going beyond what is feasible in postmortem studies, our in vivo approach allowed us to relate macro- and microstructural measures of PT architecture to a functional measure of auditory speech processing. To test whether interindividual differences in the neurophysiological correlates of auditory speech perception are modulated by PT architecture, we correlated the macro- and microstructural properties of the PT with the N1 latencies during the dichotic listening task. We focused our analysis on the N1 latency because the dominance of the left PT for fast temporal processing has been suggested to underlie language lateralization (*6*).

For PT volume, we did not find any significant association with N1 latencies during the dichotic condition (table S1) or noise condition (table S4). This lack of association between PT macrostructure and auditory speech processing is in line with previous results (*25*) and further supports the assumption that macrostructural asymmetries of the PT are not the structural basis of functional asymmetries.

However, PT neurite architecture asymmetries significantly predicted N1 latency. INVF of the left PT showed a significant negative correlation with left hemispheric N1 latency ($r = -0.25$, $P < 0.05$) (Fig. 3 and Table 1), indicating that individuals with higher neurite density in the left PT showed shorter N1 latencies in the left hemisphere. Other structure-function relationships between NODDI measures and neurophysiological correlates during the dichotic (tables S2 and S3) or noise condition (tables S5 to S7) were not significant.

Finally, we conducted a multiple regression analysis. In doing so, we were able to extract the unique contribution of each macro- and microstructural brain property of the left PT in predicting N1 latency in the left hemisphere. In a combined multiple regression analysis with INVF, ODI, ISO, and VOL of the left PT as predictors and N1 latency in the left hemisphere as the dependent variable, INVF of the left PT was the only variable providing a unique contribution in predicting N1 latency in the left hemisphere ($\beta = -0.23$; $P < 0.05$; other predictors, all $P > 0.11$; see Table 2). An alternative regression model including sex and estimates of handedness (laterality quotient) as additional predictors did not change the pattern of results (table S8).

One potential confounding factor in our model could be cortical thickness. If the left PT had thicker gray matter, it would be less susceptible to partial volume with subcortical white matter that might modulate asymmetries in neurite density and orientation dispersion of PT. To rule out this possibility, we tested asymmetries in cortical thickness of the PT in the left hemisphere. We did not find a significant cortical thickness difference for the PT between the two hemispheres (left PT: 2.58 ± 0.15 mm; right PT: 2.59 ± 0.17 mm;

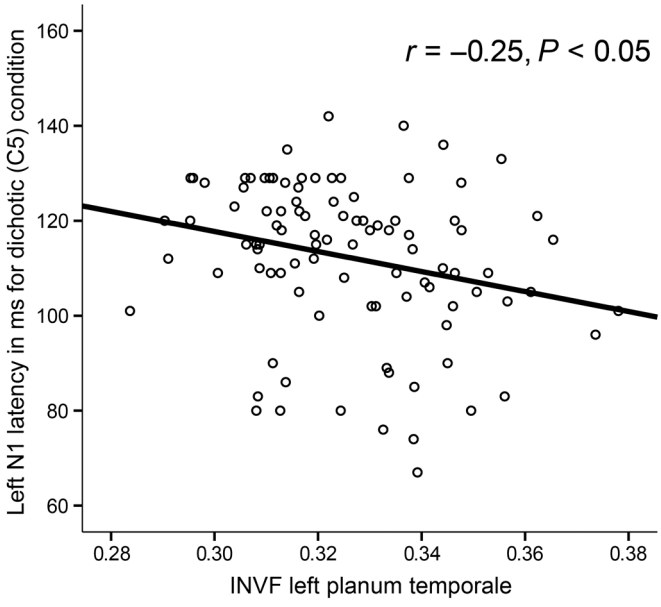

Fig. 3. Association between auditory speech processing and neurite architecture. Scatter plot illustrating the relationship between INVF of the left PT and N1 latency of the left electrode (C5).

$t_{97} = -0.71$; $P = 0.48$). In addition, we calculated a second alternative regression model including cortical thickness and NODDI coefficient predictors. The inclusion of cortical thickness did not change the pattern of results for neurite density (table S9).

EEG signals are assumed to be driven by postsynaptic potentials from apical dendrites of cortical neurons and not from action potentials of long-range fibers. We nevertheless aimed to rule out the possibility that structural properties of long-range association fibers might affect our results. The source reconstruction areas displayed in Fig. 1B overlapped with the location of the arcuate fasciculus (AF), the main association fiber tract in the language system. Because this fiber tract has been proposed to play an important role for functional hemispheric asymmetries in the language system (*26*), we conducted fiber tracking of the AF (see Materials and Methods) and calculated correlations between macrostructure (volume) and NODDI coefficients of the AF and EEG measures (see tables S10 to S13). There were no significant associations. This finding supports the idea that our EEG measures were mostly determined by gray, and not white, matter structure.

DISCUSSION

The major aim of our study was to investigate the specific relationship between microstructural PT architecture and the neurophysiological correlates of auditory speech processing in order to develop a mechanistic account on the superiority of the left hemisphere in the temporal domain that gives rise to language dominance. Our results demonstrate that the left PT shows a higher density of dendrites and axons, which also display a higher degree of arborization. Neurite density of the left PT significantly predicts N1 latency in the left hemisphere. This effect was highly specific and not affected by macrostructural measures of the PT, such as cortical volume or thickness. Moreover, macro- and microstructural properties of the AF were not associated with N1 latency in the left hemispheres, indicating that specifically gray matter microstructure, and not potentially relevant white matter tracts, affects the EEG signal.

Table 1. Correlations between INVF of the PT and N1 latency during dichotic condition. *P* values are two-tailed and Bonferroni-corrected for multiple comparisons.

	INVF left PT	INVF right PT
Left N1 latency dichotic (C5)	$r = -0.25$, $P < 0.05$	$r = -0.07$, $P = 0.99$
Right N1 latency dichotic (C6)	$r = 0.00$, $P = 0.99$	$r = 0.05$, $P = 0.99$

Nearly a hundred years of postmortem human brain samples that span close to a century could demonstrate that area PT is characterized by long vertical columns of closely apposed somata with a width of just a few cell bodies (*10*, *11*, *14*). These microcolumns are equidistantly separated by neuropil. This arrangement shows a couple of morphological asymmetries. Left PT microcolumns are wider and are located farther away from the next one (*10*). As a consequence, dendrites of neurons in neighboring microcolumns overlap less on the left (*12*, *13*). In addition, left PT microcolumns are innervated by a higher density of axons, and these axons are more spatially localized and thus innervate a smaller number of microcolumns (*12*, *27*). Finally, left microcolumns are connected to a larger number of other microcolumns than those on the right.

Our in vivo results extend the insights of these studies and connect them to physiological measures of speech processes. As a consequence, we can derive a working hypothesis on how the microstructure of left hemispheric PT could promote a high temporal precision of spiking subsequent to speech input (Fig. 4).

We observed a significantly higher density of dendrites and axons in the left PT. Postmortem Golgi studies of human PT described higher axonal densities in left microcolumns, a higher degree of single axon-to-microcolumn mappings on the left, and an absence of overlapping dendritic space between neighboring microcolumns in the left hemisphere (*12*, *27*).

The human auditory cortex shows a clear tonotopic columnar sound frequency organization that is stable through cortical depth (*28*). As a result, we would expect that a high number of left hemispheric axons that transmit a frequency-specific volley of spikes on a large number of dendrites along the length of a microcolumn could cause a near-synchronous activation of columnar neurons. Concerted presynaptic firing can result in strong membrane depolarization and a reduced membrane time constant such that neurons produce tightly phase-locked spikes and turn into better coincidence detectors (*29*–*31*). This could increase temporal precision and, importantly, decrease the latency of left PT neurons. Our ERP data support the idea that such a synchronous mass potential in the left PT may underlie leftward dominance for auditory speech processing, as this area was localized as the source of the N1. However, when interpreting these results, it has to be considered that NODDI-derived neurite density as reflected by INVF might be, in part, influenced by myelin (*32*, *33*) and that postmortem studies indicate that the left posterior superior temporal lobe shows a significant leftward myelination asymmetry (*34*). Because myelination is also a microstructural feature of relevance to processing speed, future studies should investigate the link between myelin, NODDI metrics, and

Table 2. Multiple regression analysis predicting left N1 latency during dichotic condition by structural predictors.

Predictors	β	*t*	*P*
Left PT INVF	−0.23	−2.34	0.02
Left PT ODI	0.10	0.99	0.32
Left PT ISO	0.13	1.34	0.18
Left PT VOL	0.15	1.50	0.14
Dependent variable: left N1 latency dichotic (C5)		$R^2 = 0.11$, $P = 0.024$	

neurophysiological processing in greater detail. Together, our NODDI-EEG results are possibly part of a mechanistic account on how microstructural properties of the left PT could produce the hemispheric difference that drives language dominance due to left-right differences of time advantage and higher temporal resolution.

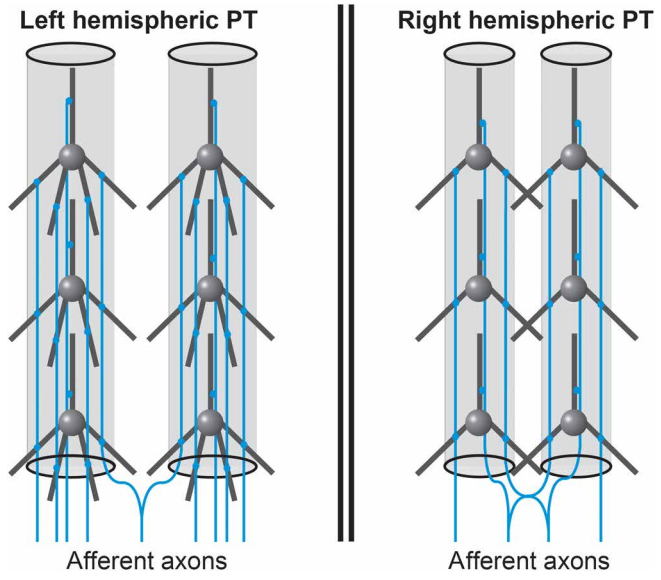

Fig. 4. Hypothetical model of the microstructural asymmetries of human area PT as revealed by current in vivo study. Highly schematized depiction of two microcolumns in left and right hemispheric PT. The density of dendrites and axons is higher on the left. In addition, left PT neurons have a higher degree of arborization. On the basis of previously published postmortem data, microcolumns are wider and further apart in the left hemisphere such that dendritic arbors do not overlap. Furthermore, afferents axons innervate smaller numbers of neighboring microcolumns, possibly enabling sharper tonotopic mapping of columnar frequencies. The higher density of dendrites and afferents on the left side could enable near-synchronous activation of frequency-specific microcolumnar neurons, thereby decreasing the latency of left PT cells and increasing their temporal precision.

MATERIALS AND METHODS

Participants

One hundred two participants aged between 18 and 33 years (mean age, 23.63 years; 54 males) were tested in the present study. Seventy participants were right-handed (mean laterality quotient, 84.30; SD, 21.21), and the remaining 32 participants were left-handed (mean laterality quotient, −73.28; SD, 24.75). Handedness was measured with the Edinburgh Handedness Inventory (EHI) (*35*). Participants had no history of neurological or psychiatric disorders and matched the standard inclusion criteria for functional MRI (fMRI) examinations. Before the beginning of the experiment, participants' hearing capabilities were tested using audiometric screening at 6000, 3000, 1500, and 750 Hz. None of the individuals included in our final sample had any interaural differences of more than 15 dB for any of these frequencies.

Because of technical difficulties with the EEG acquisition, four individuals were excluded from the study. Thus, the final sample consisted of 98 participants (mean age, 23.62 years; SD, 3.58; 52 males, 46 females). The study was approved by the relevant ethics authority (the local ethics committee of the Faculty of Psychology at Ruhr-University Bochum). All participants had to give written informed consent and were treated in accordance with the Declaration of Helsinki. Participants either were paid or received course credit. Two testing sessions took place.

In the first session, handedness was assessed and participants were tested with the EEG dichotic listening task. In the second session, all MRI imaging was performed at the Bergmannsheil Hospital in Bochum.

EEG dichotic listening paradigm

The EEG dichotic listening paradigm was used and validated in two previous studies by (*24*, *36*). The paradigm was a passive dichotic listening task, with the stimuli consisting of six consonant-vowel syllable pairs (for example, "BA," "DA," "GA," "KA," "PA," and "TA"). Stimuli were spoken by an adult German male and had a duration of 350 ms. The stimulus set was pretested and validated in a previous study on *GRIN2B* gene variation and dichotic listening (*37*). Stimuli were presented at 30 dB via earphones using Presentation software (Neurobehavioral Systems Inc.). Voice onset time differences between voiced consonants such as "BA," "DA," and "GA" and voiceless consonants such as "KA," "PA," and "TA" were controlled for. Spectral temporal envelopes of the different stimuli were matched.

Before the beginning of the experiment, participants were told to passively listen to the stimuli. There were two different conditions. In the "dichotic condition," two different stimuli (such as "GA" and "TA") were played simultaneously, one to each ear. To prevent any confounding effects of syllable type, all possible combinations of syllable pairs were presented in a counterbalanced manner. The second condition was the "noise condition," in which white noise was presented to both ears instead of the verbal stimulus material that was used in the dichotic condition. This condition was included as a control condition to ensure that the results of the dichotic listening condition reflected a specific effect of language lateralization, rather than a nonspecific auditory phenomenon. The paradigm began with a 10-trial training block that was excluded from further analysis. Afterward, three experimental blocks consisting of 30 dichotic trials and 30 noise trials were administered. Thus, overall, the paradigm consisted of 180 trials, with 90 trials for both the dichotic and the noise condition. Stimulus order was randomized, and the interstimulus interval was randomized between 3150 and 3650 ms to avoid habituation effects.

Recording and analysis of EEG signals

During the passive dichotic listening task, EEG signals were recorded with a sampling rate of 1000 Hz using a Brain Products actiCAP setup with 64 active electrodes at standard scalp positions. FCz was used as the reference electrode, and the impedance of all electrodes was below 5 kilohms. EEG data were analyzed using Brain Vision

Analyser II software (Brain Products). Raw data were first filtered with a band-pass (IIR) filter (0.5 to 20 Hz). Several measures were taken to control for or reject artifacts. First, the filtered EEG was visually inspected for large technical artifacts (for example, head or jaw movements), or faulty channels, which were removed from the following analysis. Subsequently, recurrent, physiological artifacts, such as eye blinks, saccades, or pulse, were excluded using an independent component analysis (ICA) approach. ICA was performed using the infomax algorithm, and all ICA components reflecting the aforementioned artifacts were excluded from further analysis. Afterward, FCz and all excluded channels were interpolated topographically with spherical splines. Stimulus-locked segmentation (from −100 ms before to 500 ms after stimulus presentation) was performed for all conditions. Subsequently, automated artifact rejection was performed for each segment. If a maximal amplitude difference of 200 (μV) in a 100-ms interval or activity below 0.5 (μV) in a 200-ms period was observed in any electrode, then the segment was excluded from further analysis. This procedure led to the rejection of less than 1% of all trials.

Subsequently, baseline correction −100 ms to stimulus onset was performed, and the average signal for each channel was determined. N1 peak detection was performed at electrodes C5 (left) and C6 (right), which were previously shown to generate reliable N1 responses, both in dichotic listening (*36*). N1 amplitude and latency of the N1 peak were used as dependent variables for further analysis and thus were extracted for both electrodes.

Standardized low-resolution brain electromagnetic tomography

To reconstruct the cortical distribution of source locations contributing to the N1 ERP component during dichotic listening, we used sLORETA (*23*). sLORETA is an upgraded version of LORETA (*38*). It determines a single linear solution for the inverse problem of brain function source localization without any localization bias (*39*). The accuracy of sLORETA was validated by TMS (transcranial magnetic stimulation)/EEG studies (*40*) and by simultaneous EEG/fMRI studies (*41*). For visualization purposes, we used a three-dimensional head model that was based on the MNI152 template (*42*). Overall, the model consisted of 6239 voxels with a spatial resolution of 5 mm. For each of these voxels, standardized current density was determined. Statistical analyses were performed using voxel-wise randomization tests that were based on SnPM. The number of permutations was set to 5000. On the basis of the EEG signal in the dichotic condition, one-sample *t* tests were used to localize the source of EEG amplitudes. The sLORETA viewer was then used to determine all voxels that showed a significant difference from zero with $P < 0.01$ (corrected for multiple comparisons) and their MNI coordinates.

Acquisition of imaging data

All imaging data were acquired at the Bergmannsheil Hospital in Bochum, Germany, using a 3T Philips Achieva scanner with a 32-channel head coil.

Anatomical imaging

For the purpose of segmenting brain scans into gray and white matter sections, as well as for the identification of anatomical landmarks, a T1-weighted high-resolution anatomical image was acquired [MP-RAGE; TR (repetition time), 8179 ms; TE (echo time), 3.7 ms; flip angle, 8°; 220 slices; matrix size, 240 × 240; resolution, 1 × 1 × 1 mm]. The acquisition time of the anatomical image was 6 min.

Diffusion-weighted imaging for NODDI

For the analysis of NODDI coefficients, diffusion-weighted images were acquired using echo planar imaging (TR, 7652 ms; TE, 87 ms; flip angle, 90°; 60 slices; matrix size, 112 × 112; resolution, 2 × 2 × 2 mm). Diffusion weighting was based on a multishell, high-angular-resolution scheme consisting of diffusion-weighted images for *b* values of 1000, 1800, and 2500 s/mm^2, respectively, applied along 20, 40, and 60 uniformly distributed directions. All diffusion directions within and between shells were generated orthogonal to each other using the MASSIVE toolbox (*43*). In addition, eight data sets with no diffusion weighting ($b = 0$ s/mm^2) were acquired as an anatomical reference for motion correction and computation of NODDI coefficients. The acquisition time of the diffusion-weighted images was 18 min.

Diffusion-weighted imaging for fiber tracking

Because the AF was proposed to play an important role for functional hemispheric asymmetries in the language system (*26*), we additionally recorded conventional diffusion tensor images of our participants. All diffusion-weighted images were collected with the following parameters: TR, 7652 ms; TE, 87 ms; flip angle, 90°; 80 slices; matrix size, 112 × 112; resolution, 2 × 2 × 2 mm. To increase signal-to-noise ratio, three consecutive single-shot spin-echo echo-planar images were subsequently averaged. Diffusion weighting was isotropically distributed along 60 directions. Except for six non–diffusion-weighted images, all images were acquired with a *b* value of 1000 s/mm^2. The six nonweighted images ($b = 0$ s/mm^2) were used for anatomical reference and motion correction. The acquisition time of the diffusion-weighted images was 36 min.

Analysis of imaging data

Anatomical data

The cortical surfaces of the T1-weighted images were reconstructed using FreeSurfer (http://surfer.nmr.mgh.harvard.edu, version 5.3.0). The details of this procedure were explained in detail elsewhere (*44*). The automatic reconstruction steps involved skull stripping, gray and white matter segmentation, and reconstruction and inflation of the cortical surface. These processing steps were performed for each participant individually. After preprocessing, each segmentation was quality-controlled slice by slice. Inaccuracies for the automatic steps were corrected by manual editing, if necessary. Because the PT has a pivotal role in auditory speech processing (*7*), we defined this area per hemisphere from the T1-weighted anatomical using an automatic segmentation procedure implemented in FreeSurfer (Fig. 1). Here, the PT was extracted following a gyral/sulcal-based parcellation algorithm from the Destrieux atlas (*45*) and was examined with regard to structure-function relationships in terms of lateralization of auditory speech perception. Brain segmentation yielded a volume estimation of the left and right PT (VOL) (Fig. 1). Moreover, cortical thickness was also determined. The right PT was used as a control area in the analysis, as we did not expect a relation with EEG results in this area. In a final step, each PT yielded by the parcellation algorithm was linearly transformed into the native space of the diffusion-weighted images (Fig. 1). The transformed regions served as anatomical landmarks from which NODDI coefficients were extracted (Fig. 1).

NODDI diffusion data

Diffusion images were preprocessed using FDT (FMRIB's Diffusion Toolbox) as implemented in FSL version 5.0.7. Preprocessing steps included a correction for eddy currents and head motion as well as a correction of the gradient direction for each volume using the rotation

parameters that emerged from head motion. NODDI coefficients were computed using the AMICO (accelerated microstructure imaging via convex optimization) toolbox (*46*). The AMICO approach was based on a convex optimization procedure that converts the nonlinear fitting into a linear optimization problem (*46*). This framework allows robust estimation of multiple fiber populations and microstructural NODDI indices by markedly reducing processing tie (*47*). Data analysis with NODDI can be applied to cortical regions and white matter structures. The technique was based on a two-level approach and featured a three-compartment model distinguishing intraneurite, extraneurite, and cerebrospinal environments. First, the diffusion signal obtained by the multishell, high-angular-resolution imaging protocol was used to determine the proportion of free-moving water within each voxel (*15*–*17*, *19*, *46*). This ratio is termed isotropic volume fraction (ISO) and reflects the amount of isotropic diffusion with Gaussian properties likely to be found in the cerebrospinal fluid of gray and white matter regions. Second, the remaining portion of the diffusion signal is divided into the INVF and the extraneurite volume fraction. Here, by definition, the two volume fractions representing intra- and extraneurite diffusion complement each other and add up to 1 (*15*–*17*). INVF represents the amount of stick-like or cylindrically symmetric diffusion that is created when water molecules are restricted by the membranes of neurites. In white matter structures, this kind of diffusion is likely to resemble the proportion of axons. In gray matter regions, it serves as an indicator of dendrites and axons forming the neuropil. Extraneurite volume fraction is based on hindered diffusion within extraneurite environments, which are usually occupied by various types of glial cells in white matter structures and both neurons and glial cells in gray matter regions (*15*–*17*).

Neurite orientation dispersion (ODI) is a tortuosity measure coupling the intraneurite space and the extraneurite space, resulting in alignment or dispersion of axons in white matter or axons and dendrites in gray matter (*17*). Examples of INVF, ODI, and ISO coefficient maps from a representative individual are illustrated in Fig. 1. As described above, each PT defined for the T1-weighted anatomical scan was transformed into the native space of the diffusion-weighted images to compute NODDI coefficients for these areas.

Fiber tracking

To explore the potential role of long-range white matter fiber tracts connecting to the source reconstruction areas of our EEG analysis (see Fig. 1B), we performed fiber tracking of the AF (see fig. S1) using constrained spherical deconvolution (*48*) in ExploreDTI (www.exploredti.com/). After conventional preprocessing steps (correction for eddy currents and head motion, as well as a correction of the gradient direction for each volume using the rotation parameters that emerged from head motion), whole-brain tractography of each subject was performed. In the second step, we used two-dimensional gates "AND" and "NOT" to extract fiber tracts belonging to the AF in the left and right hemisphere. The gates for delineating AF were chosen in accordance to the *Atlas of Human Brain Connections* (*49*). All steps were performed in native diffusion space by an individual, which was blind to the neurophysiological results of this study. In a final step, AF in each hemisphere was linearly transformed into the native space of the NODDI images to compute the volume and the three NODDI coefficients for these tracts.

Statistical analysis

Statistical analyses were carried out using MATLAB version 7.14.0.739 (R2012a, MathWorks Inc.) and SPSS version 20 (SPSS Inc.). Linear parametric methods were used for all analyses. The α level was set to 0.05 (two-tailed). To control for multiple comparisons, Bonferroni correction was used if necessary.

Analysis of variance

N1 latencies and amplitudes were analyzed using two-way (2×2) repeated-measures ANOVAs with the following within-participant factors: hemisphere (left or right) and condition (dichotic or noise). Subsequent post hoc tests were Bonferroni-corrected with a factor of 4.

Correlation analysis

We examined structure-function relationships by computing Pearson's linear correlation coefficients between the neurophysiological correlates during the dichotic listening task and the structural brain properties of the PT and AF included in this study (VOL, INVF, ODI, and ISO).

Multiple regression analysis

To examine the aforementioned structure-function relationships with regard to the unique contribution of each NODDI estimate of the PT, we computed an inclusion/enter multiple regression analysis using SPSS. The neurophysiological correlate during the dichotic listening task was treated as the dependent variable, and INVF, ODI, and ISO were treated as predictors.

SUPPLEMENTARY MATERIALS

Supplementary material for this article is available at http://advances.sciencemag.org/cgi/content/full/4/7/eaar6830/DC1

Table S1. Correlations between VOL of PT and N1 latency during dichotic condition.
Table S2. Correlations between ODI of PT and N1 latency during dichotic condition.
Table S3. Correlations between ISO of PT and N1 latency during dichotic condition.
Table S4. Correlations between VOL of PT and N1 latency during noise condition.
Table S5. Correlations between INVF of PT and N1 latency during noise condition.
Table S6. Correlations between ODI of PT and N1 latency during noise condition.
Table S7. Correlations between ISO of PT and N1 latency during noise condition.
Table S8. Multiple regression analysis (alternative model 1) predicting left N1 latency during dichotic condition by structural predictors.
Table S9. Multiple regression analysis predicting left N1 latency during dichotic condition by structural predictors.
Table S10. Correlations between VOL of AF and N1 latency during dichotic condition.
Table S11. Correlations between INVF of AF and N1 latency during dichotic condition.
Table S12. Correlations between ODI of AF and N1 latency during dichotic condition.
Table S13. Correlations between ISO of AF and N1 latency during dichotic condition.
Fig. S1. Sagittal view of the left AF.

REFERENCES AND NOTES

1. M. C. Corballis, Lateralization of the human brain. *Prog. Brain Res.* **195**, 103–121 (2012).
2. K. Hugdahl, Lateralization of cognitive processes in the brain. *Acta Psychol.* **105**, 211–235 (2000).
3. B. Mazoyer, L. Zago, G. Jobard, F. Crivello, M. Joliot, G. Perchey, E. Mellet, L. Petit, N. Tzourio-Mazoyer, Gaussian mixture modeling of hemispheric lateralization for language in a large sample of healthy individuals balanced for handedness. *PLOS ONE* **9**, e101165 (2014).
4. M. L. Concha, I. H. Bianco, S. W. Wilson, Encoding asymmetry within neural circuits. *Nat. Rev. Neurosci.* **13**, 832–843 (2012).
5. N. Tzourio-Mazoyer, M. Perrone-Bertolotti, G. Jobard, B. Mazoyer, M. Baciu, Multi-factorial modulation of hemispheric specialization and plasticity for language in healthy and pathological conditions: A review. *Cortex* **86**, 314–339 (2017).
6. R. J. Zatorre, P. Belin, Spectral and temporal processing in human auditory cortex. *Cereb. Cortex* **11**, 946–953 (2001).
7. J. Shapleske, S. L. Rossell, P. W. R. Woodruff, A. S. David, The planum temporale: A systematic, quantitative review of its structural, functional and clinical significance. *Brain Res. Brain Res. Rev.* **29**, 26–49 (1999).
8. N. Geschwind, W. Levitsky, Human brain: Left-right asymmetries in temporal speech region. *Science* **161**, 186–187 (1968).
9. A. M. Galaburda, M. LeMay, T. L. Kemper, N. Geschwind, Right-left asymmetrics in the brain. *Science* **199**, 852–856 (1978).

10. C. von Economo, L. Horn, Über Windungsrelief, Maße und Rindenarchitektonik der Supratemporalfläche, ihre individuellen und ihre Seitenunterschiede. *Z. Neurol. Psychiat.* **130**, 687–757 (1930).
11. H. L. Seldon, Structure of human auditory cortex. I. Cytoarchitectonics and dendritic distributions. *Brain Res.* **229**, 277–294 (1981).
12. H. L. Seldon, Structure of human auditory cortex. II. Axon distributions and morphological correlates of speech perception. *Brain Res.* **229**, 295–310 (1981).
13. H. L. Seldon, Structure of human auditory cortex. III. Statistical analysis of dendritic trees. *Brain Res.* **249**, 211–221 (1982).
14. R. A. W. Galuske, W. Schlote, H. Bratzke, W. Singer, Interhemispheric asymmetries of the modular structure in human temporal cortex. *Science* **289**, 1946–1949 (2000).
15. S. N. Jespersen, C. R. Bjarkam, J. R. Nyengaard, M. M. Chakravarty, B. Hansen, T. Vosegaard, L. Østergaard, D. Yablonskiy, N. C. Nielsen, P. Vestergaard-Poulsen, Neurite density from magnetic resonance diffusion measurements at ultrahigh field: Comparison with light microscopy and electron microscopy. *Neuroimage* **49**, 205–216 (2010).
16. S. N. Jespersen, L. A. Leigland, A. Cornea, C. D. Kroenke, Determination of axonal and dendritic orientation distributions within the developing cerebral cortex by diffusion tensor imaging. *IEEE Trans. Med. Imaging* **31**, 16–32 (2012).
17. H. Zhang, T. Schneider, C. A. Wheeler-Kingshott, D. C. Alexander, NODDI: Practical in vivo neurite orientation dispersion and density imaging of the human brain. *Neuroimage* **61**, 1000–1016 (2012).
18. L. Alonso-Nanclares, J. Gonzalez-Soriano, J. R. Rodriguez, J. DeFelipe, Gender differences in human cortical synaptic density. *Proc. Natl. Acad. Sci. U.S.A.* **105**, 14615–14619 (2008).
19. F. Grussu, T. Schneider, C. Tur, R. L. Yates, M. Tachrount, A. Ianuş, M. C. Yiannakas, J. Newcombe, H. Zhang, D. C. Alexander, G. C. DeLuca, C. A. M. Gandini Wheeler-Kingshott, Neurite dispersion: A new marker of multiple sclerosis spinal cord pathology? *Ann. Clin. Transl. Neurol.* **4**, 663–679 (2017).
20. G. Grossi, N. Savill, E. Thomas, G. Thierry, Posterior N1 asymmetry to English and Welsh words in Early and Late English-Welsh bilinguals. *Biol. Psychol.* **85**, 124–133 (2010).
21. C. Spironelli, A. Angrilli, Developmental aspects of automatic word processing: Language lateralization of early ERP components in children, young adults and middle-aged subjects. *Biol. Psychol.* **80**, 35–45 (2009).
22. C. S. Herrmann, R. T. Knight, Mechanisms of human attention: Event-related potentials and oscillations. *Neurosci. Biobehav. Rev.* **25**, 465–476 (2001).
23. R. D. Pascual-Marqui, Standardized low-resolution brain electromagnetic tomography (sLORETA): Technical details. *Methods Find. Exp. Clin. Pharmacol.* **24**, 5–12 (2002).
24. P. Friedrich, S. Ocklenburg, N. Heins, C. Schlüter, C. Fraenz, C. Beste, O. Güntürkün, E. Genç, Callosal microstructure affects the timing of electrophysiological left-right differences. *Neuroimage* **163**, 310–318 (2017).
25. D. N. Greve, L. Van der Haegen, Q. Cai, S. Stufflebeam, M. R. Sabuncu, B. Fischl, M. Brysbaert, A surface-based analysis of language lateralization and cortical asymmetry. *J. Cogn. Neurosci.* **25**, 1477–1492 (2013).
26. S. Ocklenburg, P. Friedrich, O. Güntürkün, E. Genç, Intrahemispheric white matter asymmetries: The missing link between brain structure and functional lateralization? *Rev. Neurosci.* **27**, 465–480 (2016).
27. H. L. Seldon, The anatomy of speech perception, in *Association and Auditory Cortices*, A. Peters, E. G. Jones, Eds. (Springer, 1985), pp. 273–327.
28. F. de Martino, M. Moerel, K. Ugurbil, R. Goebel, E. Yacoub, E. Formisano, Frequency preference and attention effects across cortical depths in the human primary auditory cortex. *Proc. Natl. Acad. Sci. U.S.A.* **112**, 16036–16041 (2015).
29. A. Destexhe, M. Rudolph, D. Paré, The high-conductance state of neocortical neurons in vivo. *Nat. Rev. Neurosci.* **4**, 739–751 (2003).
30. J. F. A. Poulet, C. C. H. Petersen, Internal brain state regulates membrane potential synchrony in barrel cortex of behaving mice. *Nature* **454**, 881–885 (2008).
31. D. B. Salkoff, E. Zagha, Ö. Yüzgeç, D. A. McCormick, Synaptic mechanisms of tight spike synchrony at gamma frequency in cerebral cortex. *J. Neurosci.* **35**, 10236–10251 (2015).
32. M. Kleinnijenhuis, *Imaging Fibres in the Brain* (Donders Institute for Brain, Cognition and Behaviour, 2014).
33. M. Kleinnijenhuis, H. Zhang, D. Wiedermann, D. G. Norris, A.-M. Van Cappellen van Walsum, Detailed laminar characteristics of the human neocortex revealed by NODDI and histology, in *Annual Meeting of the Organization for Human Brain Mapping*, Seattle, WA (Organization for Human Brain Mapping, 2013), p. 3815.
34. B. Anderson, B. D. Southern, R. E. Powers, Anatomic asymmetries of the posterior superior temporal lobes. *Neuropsychiatry Neuropsychol. Behav. Neurol.*. **12**, 247–254 (1999).
35. R. C. Oldfield, The assessment and analysis of handedness: The Edinburgh inventory. *Neuropsychologia* **9**, 97–113 (1971).
36. C. Beste, S. Ocklenburg, M. von der Hagen, N. Di Donato, Mammalian cadherins DCHS1-FAT4 affect functional cerebral architecture. *Brain Struct. Funct.* **221**, 2487–2491 (2016).
37. S. Ocklenburg, L. Arning, C. Hahn, W. M. Gerding, J. T. Epplen, O. Güntürkün, C. Beste, Variation in the NMDA receptor 2B subunit gene GRIN2B is associated with differential language lateralization. *Behav. Brain Res.* **225**, 284–289 (2011).
38. R. D. Pascual-Marqui, C. M. Michel, D. Lehmann, Low resolution electromagnetic tomography: A new method for localizing electrical activity in the brain. *Int. J. Psychophysiol.* **18**, 49–65 (1994).
39. K. Sekihara, M. Sahani, S. S. Nagarajan, Localization bias and spatial resolution of adaptive and non-adaptive spatial filters for MEG source reconstruction. *Neuroimage* **25**, 1056–1067 (2005).
40. G. Dippel, C. Beste, A causal role of the right inferior frontal cortex in implementing strategies for multi-component behaviour. *Nat. Commun.* **6**, 6587 (2015).
41. S. Olbrich, C. Mulert, S. Karch, M. Trenner, G. Leicht, O. Pogarell, U. Hegerl, EEG-vigilance and BOLD effect during simultaneous EEG/fMRI measurement. *Neuroimage* **45**, 319–332 (2009).
42. J. Mazziotta, A. Toga, A. Evans, P. Fox, J. Lancaster, K. Zilles, R. Woods, T. Paus, G. Simpson, B. Pike, C. Holmes, L. Collins, P. Thompson, D. MacDonald, M. Iacoboni, T. Schormann, K. Amunts, N. Palomero-Gallagher, S. Geyer, L. Parsons, K. Narr, N. Kabani, G. Le Goualher, D. Boomsma, T. Cannon, R. Kawashima, B. Mazoyer, A probabilistic atlas and reference system for the human brain: International Consortium for Brain Mapping (ICBM). *Philos. Trans. R. Soc. Lond. B Biol. Sci.* **356**, 1293–1322 (2001).
43. M. Froeling, C. M. W. Tax, S. B. Vos, P. R. Luijten, A. Leemans, "MASSIVE" brain dataset: Multiple acquisitions for standardization of structural imaging validation and evaluation. *Magn. Reson. Med.* **77**, 1797–1809 (2017).
44. B. Fischl, M. I. Sereno, A. M. Dale, Cortical surface-based analysis. II: Inflation, flattening, and a surface-based coordinate system. *Neuroimage* **9**, 195–207 (1999).
45. C. Destrieux, B. Fischl, A. Dale, E. Halgren, Automatic parcellation of human cortical gyri and sulci using standard anatomical nomenclature. *Neuroimage* **53**, 1–15 (2010).
46. A. Daducci, E. J. Canales-Rodríguez, H. Zhang, T. B. Dyrby, D. C. Alexander, J. P. Thiran, Accelerated Microstructure Imaging via Convex Optimization (AMICO) from diffusion MRI data. *Neuroimage* **105**, 32–44 (2015).
47. F. Sepehrband, D. C. Alexander, N. D. Kurniawan, D. C. Reutens, Z. Yang, Towards higher sensitivity and stability of axon diameter estimation with diffusion-weighted MRI. *NMR Biomed.* **29**, 293–308 (2016).
48. J.-D. Tournier, F. Calamante, A. Connelly, Robust determination of the fibre orientation distribution in diffusion MRI: Non-negativity constrained super-resolved spherical deconvolution. *Neuroimage* **35**, 1459–1472 (2007).
49. M. Catani, M. Thiebaut de Schotten, *Atlas of Human Brain Connections* (Oxford Univ. Press, 2012).

Acknowledgments: We thank C. Koch for help with the fiber tracking of the AF. We also thank L. Schlaffke, M. Froeling, and B. Mädler (Philips Germany) for scientific support with the MRI measurements, as well as T. Otto for technical support. **Funding:** This work was supported by Deutsche Forschungsgemeinschaft (DFG) grant nos. Gu227/16-1, BE4045/26-1, and GE2777/2-1; DFG SFB 1280 project A03; and Mercur Foundation grant no. An-2015-0044. **Author contributions:** S.O., P.F., O.G., and E.G. conceived the project and supervised the experiments. S.O., O.G., and E.G. designed the experiments. C.F., C.S., and P.F. performed the experiments. P.F., C.F., C.B., and E.G. analyzed the data. S.O., C.B., O.G., and E.G. wrote the manuscript, and all authors edited the manuscript. **Competing interests:** The authors declare that they have no competing interests. **Data and materials availability:** All data reported in this paper are available from E.G. (erhan.genc@rub.de).

Submitted 6 December 2017
Accepted 31 May 2018
Published 11 July 2018
10.1126/sciadv.aar6830

Citation: S. Ocklenburg, P. Friedrich, C. Fraenz, C. Schlüter, C. Beste, O. Güntürkün, E. Genç, Neurite architecture of the planum temporale predicts neurophysiological processing of auditory speech. *Sci. Adv.* **4**, eaar6830 (2018).